The chromokinesin Kid (KIF22) forms a homodimer, moves processively along microtubules and transports double-strand DNA

Shinsuke Niwa[1,2,4,#], Natsuki Furusaki[2, 4], Tomoki Kita[2] , Yuki Suzuki[3] and Kyoko Chiba[1,#]

1 Frontier Research Institute for Interdisciplinary Sciences (FRIS), Tohoku University, Miyagi 980-0845, Japan.

2 Graduate School of Life Sciences, Tohoku University, Miyagi 980-8577, Japan.

3 Mie University, Graduate School of Engineering, 1577 Kurimamachiya-cho, 514-8507, Tsu, Japan.

4 These authors equally contributed to this work

SHINSUKE NIWA, Frontier Research Institute for Interdisciplinary Sciences (FRIS), Tohoku University, Aramaki-Aoba 6-3, Aoba-Ku, Sendai, Miyagi 980-0845, Japan.

e-mail: shinsuke.niwa.c8@tohoku.ac.jp

KYOKO CHIBA, Frontier Research Institute for Interdisciplinary Sciences (FRIS), Tohoku University, Aramaki-Aoba 6-3, Aoba-Ku, Sendai, Miyagi 980-0845, Japan.

e-mail: kyoko.chiba.e7@tohoku.ac.jp

Abstract

During prometaphase in mitosis, chromosomes are pushed toward the spindle equator. The chromokinesin Kid, also known as KIF22, moves chromosomes along spindle microtubules during prometaphase. Kid has long been considered as a monomeric and non-processive motor, different from typical kinesins. In this study, we demonstrate that the full-length Kid forms a homodimer and moves processively along microtubules. A conserved coiled-coil domain within the stalk region of Kid is not only capable of homodimer formation, but is also required for the processivity of Kid. Furthermore, the neck linker and coiled-coil domains of Kid could add processive activity to the motor domain of KIF1A, suggesting that Kid contains a functional neck linker and dimerization capability, a prerequisite for the processivity of kinesin motor domains. The full-length Kid, containing a helix-hairpin-helix domain, can transport double-strand DNA along microtubules in vitro. These findings collectively suggest the reclassification of Kid as a processive motor that transports DNA along microtubules.

Introduction

Microtubules are reorganized to form a bipolar spindle as cells enter mitosis. In the prometaphase of mitosis, chromosomes are transported along the microtubules toward the spindle equator (Rieder et al., 1986) . This process, known as chromosome congression, requires kinesin-4, kinesin-10 and kinesin-12 class of motor proteins (Bieling et al., 2010; Iemura and Tanaka, 2015; Wordeman, 2010). The mechanical forces that move chromosomes toward the spindle equator is called polar ejection forces (Brouhard and Hunt, 2005; Levesque and Compton, 2001; Rieder et al., 1986). The Kinesin-like DNA-binding protein (Kid), belonging to the kinesin-10 family and also known as KIF22, serves as a main molecular motor that transports chromosomes and generates polar ejection forces (Brouhard and Hunt, 2005; Levesque and Compton, 2001; Ohsugi et al., 2003; Thompson et al., 2022; Tokai et al., 1996; Wandke et al., 2012). Structurally, Kid contains a kinesin motor domain (Yajima et al., 2003), a coiled-coil domain (Shiroguchi et al., 2003), and a DNA binding domain (Tokai et al., 1996) (Figure 1A). In mitosis, the DNA binding domain of Kid binds along chromosome arms (Antonio et al., 2000; Funabiki and Murray, 2000; Levesque and Compton, 2001). Using the motor domain, Kid transports chromosomes (Bieling et al., 2010; Brouhard and Hunt, 2005).

A single kinesin molecule can move for hundreds of steps along a microtubule without dissociating (Hackney, 1995; Hancock and Howard, 1998). This property, called processivity, requires dimerization of kinesins (Hancock and Howard, 1998). However, Kid has long been regarded as a monomeric and non-processive motor, which can move along microtubules in only a single step (Shiroguchi et al., 2003; Yajima et al., 2003). Consistent with these findings, Kid is unique within kinesin superfamily due to lack of the conventional neck coiled-coil domain (Shiroguchi et al., 2003) , an element that determines the length of the neck linker essential for the coordinated movement of the two motor domains (Case et al., 2000; Isojima et al., 2010; Yildiz et al.,

2008). While a study has indicated the possibility that the full-length human Kid protein can move processively along microtubules (Stumpff et al., 2012), this study did not investigate the oligomeric state of Kid, nor did it provide detailed information on the Kid's motility characteristics and parameters. A Drosophila kinesin-10 motor NOD, an orthologue of Kid, is also characterized as a monomeric and non-processive motor (Matthies et al., 2001). Similar to Kid, NOD has a DNA binding domain at the tail domain (Afshar et al., 1995). NOD shows a processive movement only when the protein is forcedly dimerized by the addition of an artificial coiled-coil domain (Ye et al., 2018). Nevertheless, Kid acts as an active motor in microtubule gliding assays and cargo transport assays, both of which detect movement generated by multiple Kid motors (Bieling et al., 2010; Li et al., 2016; Shiroguchi et al., 2003; Takagi et al., 2013). Collectively, it has been widely assumed that Kid, unlike other kinesins, transports chromosomes by their cooperative action of many non-processive monomers (Brouhard and Hunt, 2005; Iemura and Tanaka, 2015; Takagi et al., 2013; Thompson et al., 2022).

Recently, we and others have analyzed properties of full-length kinesins (Chiba et al., 2022; Chiba et al., 2019; Fan, 2022; Wang et al., 2022). Notably, these studied have found that monomeric kinesins, including KIF1A, UNC-104 and KIF13B are converted to a dimer when activated (Chiba et al., 2023; Fan, 2022; Kita et al., 2024; Tomishige et al., 2002). For instance, in the autoinhibited and inactive state, KIF1A and UNC-104 are monomeric (Kita et al., 2024; Tomishige et al., 2002). The monomeric motor domain of UNC-104 and KIF1A has a plus-end directed motor activity but exhibits one-dimensional diffusion, meaning that the efficiency is low (Okada et al., 2003; Tomishige et al., 2002) . Upon the release of autoinhibition, KIF1A and UNC-104 form dimers, which exhibit efficient directional movement on microtubules (Kita et al., 2024). These studies prompted us to reanalyze the oligomeric state and the motile properties of Kid, mainly in the full length. In this study, we show that the full-length Kid protein moves processively

along microtubules. Kid proteins can form dimers but Kid proteins are dissociated to monomers at low concentrations. In the reconstitution assays in vitro, full-length Kid transport double-strand DNA along microtubules.

Results

Kid exhibits processive movement along microtubules

To study biochemical and biophysical properties of full-length Kid, we firstly purified the full-length human Kid (hKid) and Xenopus Kid (XKid) using the baculovirus system and Sf9 cells because a previous study has succeeded in purifying functional XKid from Sf9 cells (Bieling et al., 2010; Funabiki and Murray, 2000; Takagi et al., 2013). hKid as well as XKid possesses an N-terminal motor domain, a short coiled-coil domain and a DNA binding tail domain (Figure 1A). Previous studies have shown that hKid and XKid, that are fused with fluorescent proteins at the C-terminal, can complement the function of hKid-depleted cells and XKid-depleted Xenopus egg extracts (Bieling et al., 2010; Soeda et al., 2016). Thus, we fused a fluorescent protein at the C-terminal of XKid and hKid. Notably, while EGFP-fused and sfGFP-fused hKid were insoluble, mNeonGreen-fused hKid was recovered from soluble fractions. As a result, we succeeded in purifying both XKid-mScarlet and hKid-mNeonGreen proteins (Figure 1B, and supplemental Figure S1). Next, the motility of purified proteins were analyzed by single molecule motility assays using total internal reflection fluorescent microscopy (TIRF). We found that both XKid and hKid moved on microtubules processively (Figure 1C, D, Movie 1 and 2). The motility of single molecules along microtubules could be observed at 20 pM of Xkid and hKid, respectively. The average velocity of XKid and hKid were approximately 70 nm/sec (Figure 1E and Table 1), within the same range as the movement of chromosomes (Brouhard and Hunt, 2005). The run length of XKid and hKid were 4.11 ± 2.27 and 3.67 ± 2.16 μm, respectively (Figure 1F). These data collectively suggest that full-length Kid is a processive motor protein.

Full-length Kid form dimers

It has been proposed that Kid is a monomeric protein (Shiroguchi et al., 2003; Yajima et al., 2003). Even full-length human Kid protein obtained from 293T cells are indicated to be a monomer (Shiroguchi et al., 2003). However, typical kinesins show processive movement along microtubules only when they form dimers (Hancock and Howard, 1998; Kita et al., 2024; Tomishige et al., 2002). As both hKid and XKid showed processive movement on microtubules (Fig 1), we next analyzed the oligomeric state of these motors using size exclusion chromatography (Figure 2). We utilized the previously well-characterized kinesin UNC-104(1-653)-sfGFP as a size marker. UNC-104(1-653)-sfGFP exhibits a dimer peak at 200 kDa and a monomer peak at 100 kDa in size exclusion chromatography (Kita et al., 2024). This characteristic makes it a suitable marker for determining the oligomeric state of hKid and XKid, given that the predicted molecular weights of hKid-mNeonGreen and XKid-mScarlet monomers are approximately 100 kDa (Figure 1A). As a result, we found that the peak fraction of full-length hKid and XKid are almost equivalent to that of UNC-104(1-653)-sfGFP dimer (Fig 2A and B, and supplemental Figure S2). Notably, unlike UNC-104(1-653)-sfGFP, we did not detect any monomer peaks for hKid and XKid under these conditions. We next analyzed purified proteins recovered from the peak fractions using mass photometry (Sonn-Segev et al., 2020). Mass photometry is generally performed at the nanomolar concentrations (Sonn-Segev et al., 2020). Peak fractions obtained from size exclusion chromatography were diluted 100-fold and analyzed by mass photometry. The mass photometry analysis indicated the presence of significant amount of monomers (Figure 2C and D). The property is similar to the behavior of UNC-104(1-653)-sfGFP, which shows dimer peaks in the size exclusion chromatography at micromolar concentrations but dissociates into monomers at the nanomolar concentrations used for mass photometry (Kita et al., 2024). These findings indicate that full-length

hKid and XKid are capable of forming dimers, but the dimer formation is dependent on the protein concentration.

A conserved coiled-coil domain is essential for the processivity

To determine the domain essential for the processive movement of Kid, we generated a series of deletion mutants. Unfortunately, we failed to purify adequate quantities and qualities of hKid deletion mutants. Thus, following experiments were performed using XKid. We purified XKid(1-495), which lacks the DNA-binding tail domain, and XKid(1-437), which lacks the DNA-binding domain and the coiled-coil domain (Figure 3A and B, and supplemental Figure S1). Using these purified proteins, we performed single molecule motility assays (Figure 3C-F). We found XKid(1-495) could move processively on microtubules (Figure 3C). The velocity of XKid(1-495) was approximately 70 nm/sec and the run length was 4.18 ± 1.56 μm, which are comparable to those of full-length XKid (Figure 3C-F, Table 1). Thus, DNA binding domain of Kid is not required for processive runs. In contrast, XKid(1-437), which lacks the coiled-coil domain, did not show any processive runs (Figure 3D). This would be because XKid(1-437) did not form a homodimer, considering that coiled-coil domains are generally required for the dimerization of kinesins (Hancock and Howard, 1998; Kita et al., 2024). To confirm that the coiled-coil domain of XKid induces dimerization, the domain was fused with mScarlet and analyzed by the size exclusion chromatography (Figure 3G). As a result, the peak of XKidCC-mScarlet shifted to the larger size compared with that of mScarlet. The calculated molecular weight of XKidCC-mScarlet was 42 kDa, which is almost equivalent to the size of dimerized mScarlet. These data suggest that the coiled-coiled domain of Kid can induce dimer formation.

The stalk domain of XKid adds processivity to the motor domain of KIF1A

In the processive movement along the microtubules, the coordination between two motor domains is essential (Hancock and Howard, 1998). The neck linker domain, immediately following the kinesin motor domain, regulates the ATPase activity within the motor domain (Case et al., 2000). It has been shown that optimal length of the neck linker domain is crucial for achieving coordination of the two motor domains (Isojima et al., 2010; Yildiz et al., 2008). The length of the neck linker domain is typically determined by the presence of the neck coiled-coil domain (Case et al., 2000; Shastry and Hancock, 2010). However, Kid is an exception, as it does not have the conventional neck coiled-coil domain (Shiroguchi et al., 2003; Tokai et al., 1996). This unique feature of Kid supports the idea that Kid functions as a non-processive monomer (Yajima et al., 2003), which does not require the coordination between two motor domains. However, coiled-coil prediction tools might not identify hidden coiled-coil domains or Kid could have a motif that induces dimerization. In the case of kinesin-1, Alphafold2, but not coiled-coil prediction tools, can more accurately find the location of coiled-coil domains (Tan et al., 2023; Weijman et al., 2022). Therefore, we used Alphafold2 to analyze the neck-linker and the first coiled-coil domain of hKid and XKid. The result suggested that the region does not have hidden coiled-coil domains nor a motif that induces dimerization, and the region is flexible (Supplementary Figure S3). If the entire flexible region functions as a neck linker, its length is 4 times longer than that of kinesin-1 (Supplementary Figure S3) . To investigate if this extended neck linker of Kid can support the coordination of two motor domains, we fused the stalk domain of XKid to the motor domain of KIF1A (Figure 4A). We included the possible neck linker domain of XKid in this chimera protein to test whether the neck linker of XKid is functional or not (Figure 4B). We could purify the chimeric protein, named KIF1AMD-XKidSt (Figure 4C and supplementary Figure S1). We found that KIF1AMD-XKidSt exhibited processive movement along microtubules in the single molecule motility assay (Figure 4D and movie S3), as is the case of KIF1A(1-393)LZ (Figure 4E and movie S4). The velocity of

KIF1AMD-XKidSt was much faster than original XKid but slightly slower than KIF1A(1-393)LZ (Figure 4F and Table 1). The run length of KIF1AMD-XKidSt was shorter than KIF1A(1-393)LZ (Figure 4G and Table 1). Previous studies have shown that the motor domain of KIF1A does not exhibit processive motion when it is monomeric, but exhibits processive motion when an artificial dimer is generated using a stalk domain of kinesin-1 or a leucine zipper domain (Soppina et al., 2014; Tomishige et al., 2002). Therefore, these results suggest that the coiled-coil domain of XKid can induce dimerization of KIF1A motor domains on microtubules and the longer neck linker domain of XKid can support the processive movement of the kinesin motor domain.

Reconstitution of DNA transport in vitro

Kid was originally identified as a DNA binding protein (Tokai et al., 1996). The tail domain of Kid has two helix-hairpin-helix motif which is supposed to be a DNA binding domain (Doherty et al., 1996). To test that Kid has an activity to transport DNA along microtubules, we mixed fluorescently-labelled DNA in TIRF assays and directly observed the motility (Figs 5A-D). To study the domains essential for the transport of DNA, we used full-length XKid and a deletion mutant of Xkid for these assays. We found that full-length XKid can drive the movement of double-strand DNA along microtubules (Fig. 5A). Double-strand DNA signals that co-migrated with XKid were 93.4 ± 10.5 % (n = 31 microtubules). The velocity of double-strand DNA moving along microtubules was approximately 70 nm/sec, which is similar to the velocity of XKid alone (Figure 1). In contrast, single-strand DNA movement was not driven by XKid (Fig. 5B and D). Deletion of the tail domain of XKid, containing helix-hairpin-helix motif, abolished the DNA transport activity (Fig 5C and D). Finally, we confirmed that full-length hKid can induce the movement of double-strand DNA along microtubules (Supplemental Figure S4 an supplemental movie S5).

Discussion

Kid is a processive motor protein on microtubules

Prometaphase chromosomes are transported along microtubules by the activity of kinesins (Iemura and Tanaka, 2015; Wordeman, 2010). Kid is the primary kinesin that transports chromosomes along spindle microtubules in prometaphase (Brouhard and Hunt, 2005; Iemura and Tanaka, 2015). Our data show that full-length Kid is capable to form a dimer and exhibits a processive motion along microtubules, suggesting that Kid uses two motor domains and transports chromosomes along spindle microtubules as is the case in other kinesins (Figure 6A). A notable difference between this study and prior studies is the protein concentration used. Previous analysis of full-length human Kid via density gradient and size exclusion chromatography identified peak fractions through western blot, due to the low concentration of recombinant Kid expressed in 293T cells (Shiroguchi et al., 2003). We show that most hKid and XKid exist as dimers in size exclusion chromatography performed at micromolar concentrations, yet dissociate into monomers in mass photometry, which is performed at nanomolar concentrations (Figure 2). Thus, the inability to detect Kid dimers in earlier studies may be attributed to the low concentration. Another difference is the methods to detect the processivity of motors. We observed the processivity of Kid by TIRF whereas previous studies observed the motility by optical trap. In optical trapping assays, Kid is diluted prior to being adsorbed onto beads. This dilution process results in the dissociation of dimerized Kid, thereby predominantly observing the motility of monomeric Kid in the assay. Conversely, in TIRF-based motility assays, although Kid predominantly dissociates into monomers in solution, its direct interaction with microtubules leads to an increased local concentration of Kid on the microtubule surface. As a result, this would facilitate the formation of Kid dimers on the microtubules, leading to processive motility. These properties, such as "the equilibrium between monomers and dimers" and "the capability to exhibit processive movement on microtubules, even

when characterized as monomers through mass photometry" have been observed in kinesin-3 motors (Chiba et al., 2023; Fan, 2022; Kita et al., 2024).

Reconstitution of chromosome congression

A previous in vitro study, using an elegant assay termed chromatin gliding assay, has shown that XKid and XKLP1/KIF4A can crosslink between DNA and microtubules (Bieling et al., 2010). However, it remains to be elusive whether the chromosome transport is mediated by direct binding between genomic DNA and motor proteins. In the case of organelle transport, cargo adaptor proteins are generally required for efficient transport (Chiba and Niwa, 2024; Chiba et al., 2022). Our in vitro reconstitution suggests that no cargo adaptor proteins are required for Kid-dependent chromosome transport. It has been shown that Kid is regulated by phosphorylation by CDK1(Ohsugi et al., 2003). It would be interesting to study the effects of phosphorylation and dephosphorylation on the Kid-dependent DNA transport using this reconstitution system. Moreover, by extending this system, it may be possible to fully reconstitute the chromosome congression in vitro by including other kinesins and microtubule-associated proteins, such as XKLP1/KIF4A, CENP-E and NuSAP1, that are required for proper chromosome congression (Bieling et al., 2010; Iemura and Tanaka, 2015; Li et al., 2016).

Methods

Plasmids

PCR was performed using a KOD FX neo DNA polymerase (TOYOBO, Tokyo, Japan). Human Kid cDNA (corresponding to DQ895829.2) was described previously (Iemura and Tanaka, 2015). Xenopus Kid (Kif22.S, corresponding to BC070549.1) was purchased from Horizon Discovery. To generate hKidFL-mNeonGreen, DNA fragments encoding human Kid and

mNeonGreen were amplified by PCR and assembled into pFastbac1 (Novagen) by Gibson assembly as described (Gibson et al., 2009). To generate XKidFL-mScarlet, DNA fragments encoding XKid and mScarlet were amplified by PCR and assembled into pAcebac1 (Geneva Biotech). ORF sequences are shown in Supplementary Table S1. Deletion mutants of XKid were generated by PCR-based mutagenesis. For this purpose, primers were designed through the QuickChange Primer Design tool, a web-based application (Agilent). PCR-based mutagenesis was performed using KOD plus neo DNA polymerase (TOYOBO).

Expression of XKid and Kid in Sf9 cells

Sf9 cells (Thermo Fisher Scientific) were maintained in Sf900™ II SFM (Thermo Fisher Scientific) at 27°C. DH10Bac (Thermo Fisher Scientific) were transformed to generate bacmid. To prepare baculovirus, 1×10^6 cells of Sf9 cells were transferred to each well of a tissue-culture treated 6 well plate. After the cells attached to the bottom of the dishes, about ~5 μg of bacmid were transfected using 5 μL of TransIT®-Insect transfection reagent (Takara Bio Inc.). 5 days after initial transfection, the culture media were collected and spun at 3,000 × g for 3 min to obtain the supernatant (P1). For protein expression, 400 mL of Sf9 cells (2×10^6 cells/mL) were infected with 200 μL of P1 virus and cultured for 65 h at 27°C. Cells were harvested and stocked at -80°C.

Purification of proteins

We failed to purify hKid-EGFP and hKid-superfolder GFP due to the insolubility. In contrast, mNeonGreen fusion stabilized hKid and enabled purification.

Sf9 cells were resuspended in 40 mL of Kid lysis buffer (50 mM HEPES-KOH, pH 7.5, 500 mM KCH3COO, 2 mM MgSO4, 1 mM EGTA, 10% glycerol) along with 1 mM DTT, 1 mM PMSF, 0.1 mM ATP and 0.5% Triton X-100. After incubating on ice for 10 min, lysates were cleared by centrifugation (100,000 × g, 20 min, 4°C) and subjected to affinity chromatography. Lysate was

loaded on Streptactin-XT resin (IBA Lifesciences, Göttingen, Germany) (bead volume: 2 ml). The resin was washed with 40 ml Kid wash buffer (50 mM HEPES-KOH, pH 8.0, 500 mM KCH_3COO, 2 mM $MgSO_4$, 1 mM EGTA, 10% glycerol). Protein was eluted with 40 ml Kid elution buffer (50 mM HEPES-KOH, pH 8.0, 500 mM KCH_3COO, 2 mM $MgSO_4$, 1 mM EGTA, 10% glycerol, 200 mM biotin). Eluted solution was concentrated using an Amicon Ultra 15 (Merck) and then separated on an NGC chromatography system (Bio-Rad) equipped with a Superdex 200 Increase 10/300 GL column (Cytiva). Peak fractions were collected and concentrated using an Amicon Ultra 4 (Merck). Proteins were analyzed by SDS-PAGE using TGX Stain-Free gel (Bio-Rad). Concentrated proteins were aliquoted and snap-frozen in liquid nitrogen.

Mass photometry

Purified hKid and XKid obtained from the peak fractions in the SEC analysis were pooled, snap-frozen and stored until measurement. Prior to measurement, the proteins were thawed and diluted to a final concentration 5 nM in GF150 buffer (25 mM HEPES, 150 mM KCl, 2 mM $MgCl_2$, pH 7.2). Mass photometry was performed using a Refeyn OneMP mass photometer (Refeyn) and Refeyn AcquireMP version 2.3 software, with default parameters set by Refeyn AcquireMP. Bovine serum albumin (BSA) was used as a control to determine the molecular weight. The results were subsequently analyzed and graphs were prepared to visualize the data using Refeyn DiscoverMP version 2.3.

Preparation of microtubules

Tubulin was purified from porcine brain as described (Castoldi and Popov, 2003). Tubulin was labeled with Biotin-PEG_2-NHS ester (Tokyo Chemical Industry, Tokyo, Japan) and AZDye647 NHS ester (Fluoroprobes, Scottsdale, AZ, USA) as described (Al-Bassam, 2014). To polymerize

Taxol-stabilized microtubules labeled with biotin and AZDye647, 30 μM unlabeled tubulin, 1.5 μM biotin-labeled tubulin and 1.5 μM AZDye647-labeled tubulin were mixed in BRB80 buffer supplemented with 1 mM GTP and incubated for 15 min at 37°C. Then, an equal amount of BRB80 supplemented with 40 μM taxol was added and further incubated for more than 15 min. The solution was loaded on BRB80 supplemented with 300 mM sucrose and 20 μM taxol and ultracentrifuged at 100,000 g for 5 min at 30°C. The pellet was resuspended in BRB80 supplemented with 20 μM taxol.

Preparation of fluorescent-labelled DNA for the TIRF assay

Oligonucleotides labelled with Cy3 were purchased from Integrated DNA Technologies, Inc. (Coralville, Iowa, USA). Following oligonucleotides were synthesized;

Cy3-5'-GAGAATCGCCGGTTGATAATCTTCCTAGTAGGTAGTATTGGTGTTGAGTCGCTCA-3' (Oligonucleotide #1)

Cy3-5'-GAGAATCGCCGGTTGATAATCTTTGAGCGACTCAACACCAATACTACCTACTAGG-3' (Oligonucleotide #2)

Underlines indicate sequences that form double-strand DNA.

Double-strand DNA was prepared using either a VeritiPro Thermal Cycler (Applied Biosystems) or a C1000 Touch Thermal Cycler (Bio-Rad). 1 μM of Oligonucleotides #1 and #2 were mixed and subjected to the following protocol: an initial incubation at 96 °C for 2 minutes, followed by incubation at 25 °C for 1 minutes, and subsequently to 4 °C. For single-stranded DNA preparation, Oligonucleotide #1 was incubated at 96 °C and then cooled to 4 °C. Double-strand and single-strand DNA were prepared on the day of the experiment, immediately before the TIRF single-molecule motility assays. Old DNA can potentially cause high background.

TIRF single-molecule motility assays

Purified Kid proteins described above were thawed and analyzed. KIF1A (1-393)LZ, that was described in our previous work (Anazawa et al., 2022), was also thawed and reanalyzed. TIRF assays using porcine microtubules were performed as described (Chiba et al., 2019). Glass chambers were prepared by acid washing as previously described (Chiba et al., 2022). Glass chambers were coated with PLL-PEG-biotin (50% labelled, SuSoS, Dübendorf, Switzerland) and streptavidin (Wako). Polymerized microtubules were flowed into flow chambers and allowed to adhere for 5–10 min. Unbound microtubules were washed away using assay buffer (90 mM HEPES-KOH pH 7.4, 50 mM KCH_3COO, 2 mM $Mg(CH_3COO)_2$, 1 mM EGTA, 10% glycerol, 0.1 mg/ml biotin–BSA, 0.2 mg/ml kappa-casein, 0.5% Pluronic F127, 2 mM ATP, and an oxygen scavenging system composed of PCA/PCD/Trolox). Purified Kid was diluted to indicated concentrations in the assay buffer. Then, the solution was flowed into the glass chamber. An ECLIPSE Ti2-E microscope equipped with a CFI Apochromat TIRF 100XC Oil objective lens (1.49 NA), an Andor iXion life 897 camera and a Ti2-LAPP illumination system (Nikon, Tokyo, Japan) was used to observe the motility. NIS-Elements AR software ver. 5.2 (Nikon) was used to control the system. At least three independent experiments were conducted for each measurement.

Alphafold2 analysis

Alphafold2 analysis was conducted on Google Colaboratory (Jumper et al., 2021; Mirdita et al., 2022). We analyzed the amino acid sequences of KIF5C, XKid, and hKid, ranging from the neck linker to the end of coiled-coil 1. The sequences are detailed in Supplementary Table S2. The analysis was based on the assumption that these fragments form dimers and XKid and hKid fold in the similar manner.

Statistical analyses and graph preparation

Statistical analyses and graph preparation were conducted using GraphPad Prism version 10. Details on the statistical methods are provided in the figure legends. Graphs were created with GraphPad Prism version 10, exported in PDF format, and aligned using Adobe Illustrator 2023.

Acknowledgments

We would like to thank the members of Niwa lab for useful discussions. We also would like to thank Dr. Atsushi Nakagawa and Mr. Jiye Wang (Osaka University) for technical assistance. SN was supported by JSPS KAKENHI (grant no. JP23H02472). TK was supported by JSPS KAKENHI (grant no. JP23KJ0168). KC was supported by JSPS KAKENHI (grant no. JP22K15053), Uehara Memorial Foundation, Naito Foundation and MEXT Leading Initiative for Excellent Researchers (grant no. JPMXS0320200156). This work was performed under the Collaborative Research Program of Institute for Protein Research, Osaka University, CR-24-02.

Author contributions

Shinsuke Niwa: Conceptualization; Resources; Data curation; Formal analysis; Project administration; Supervision; Funding acquisition; Validation; Investigation; Visualization; Methodology; Writing—original draft; Writing—review and editing.

Natsuki Furusaki: Resources; Data curation; Formal analysis; Validation; Investigation

Tomoki Kita: Resources; Data curation; Formal analysis; Validation; Investigation

Kyoko Chiba: Resources; Data curation; Formal analysis; Supervision; Funding acquisition; Project administration; Writing—review and editing.

Conflict of interest

The authors declare no competing interests.

Statement

During the preparation of this work the authors used GPT4.0 in order to check English grammar and improve English writing. After using this tool, the authors reviewed and edited the content as needed and take full responsibility for the content of the publication.

References

Afshar, K., N.R. Barton, R.S. Hawley, and L.S. Goldstein. 1995. DNA binding and meiotic chromosomal localization of the Drosophila nod kinesin-like protein. *Cell*. 81:129-138.

Al-Bassam, J. 2014. Reconstituting Dynamic Microtubule Polymerization Regulation by TOG Domain Proteins. *Methods in Enzymology*. 540:131-148.

Anazawa, Y., T. Kita, R. Iguchi, K. Hayashi, and S. Niwa. 2022. De novo mutations in KIF1A-associated neuronal disorder (KAND) dominant-negatively inhibit motor activity and axonal transport of synaptic vesicle precursors. *Proc Natl Acad Sci U S A*. 119:e2113795119.

Antonio, C., I. Ferby, H. Wilhelm, M. Jones, E. Karsenti, A.R. Nebreda, and I. Vernos. 2000. Xkid, a chromokinesin required for chromosome alignment on the metaphase plate. *Cell*. 102:425-435.

Bieling, P., I. Kronja, and T. Surrey. 2010. Microtubule motility on reconstituted meiotic chromatin. *Curr Biol*. 20:763-769.

Brouhard, G.J., and A.J. Hunt. 2005. Microtubule movements on the arms of mitotic chromosomes: polar ejection forces quantified in vitro. *Proc Natl Acad Sci U S A*. 102:13903-13908.

Case, R.B., S. Rice, C.L. Hart, B. Ly, and R.D. Vale. 2000. Role of the kinesin neck linker and catalytic core in microtubule-based motility. *Curr Biol*. 10:157-160.

Castoldi, M., and A.V. Popov. 2003. Purification of brain tubulin through two cycles of polymerization-depolymerization in a high-molarity buffer. *Protein Expr Purif*. 32:83-88.

Chiba, K., T. Kita, Y. Anazawa, and S. Niwa. 2023. Insight into the regulation of axonal transport from the study of KIF1A-associated neurological disorder. *J Cell Sci*. 136.

Chiba, K., and S. Niwa. 2024. Autoinhibition and activation of kinesin-1 and their involvement in amyotrophic lateral sclerosis. *Curr Opin Cell Biol*. 86:102301.

Chiba, K., K.M. Ori-McKenney, S. Niwa, and R.J. McKenney. 2022. Synergistic autoinhibition and activation mechanisms control kinesin-1 motor activity. *Cell Rep*. 39:110900.

Chiba, K., H. Takahashi, M. Chen, H. Obinata, S. Arai, K. Hashimoto, T. Oda, R.J. McKenney, and S. Niwa. 2019. Disease-associated mutations hyperactivate KIF1A motility and anterograde axonal transport of synaptic vesicle precursors. *Proc Natl Acad Sci U S A*. 116:18429-18434.

Doherty, A.J., L.C. Serpell, and C.P. Ponting. 1996. The helix-hairpin-helix DNA-binding motif: a structural basis for non-sequence-specific recognition of DNA. *Nucleic Acids Res*. 24:2488-2497.

Fan, X.M., R. J. 2022. Control of motor landing and processivity by the CAP-Gly domain in the KIF13B tail. *Nat Commun*. 14:4715.

Funabiki, H., and A.W. Murray. 2000. The Xenopus chromokinesin Xkid is essential for metaphase chromosome alignment and must be degraded to allow anaphase chromosome movement. *Cell*. 102:411-424.

Gibson, D.G., L. Young, R.Y. Chuang, J.C. Venter, C.A. Hutchison, 3rd, and H.O. Smith. 2009. Enzymatic assembly of DNA molecules up to several hundred kilobases. *Nat Methods*. 6:343-345.

Hackney, D.D. 1995. Highly processive microtubule-stimulated ATP hydrolysis by dimeric kinesin head domains. *Nature*. 377:448-450.

Hancock, W.O., and J. Howard. 1998. Processivity of the motor protein kinesin requires two heads. *J Cell Biol*. 140:1395-1405.

Iemura, K., and K. Tanaka. 2015. Chromokinesin Kid and kinetochore kinesin CENP-E differentially support chromosome congression without end-on attachment to microtubules. *Nat Commun*. 6:6447.

Isojima, H., T. Mori, and M. Tomishige. 2010. Optimal Size of the Neck Linker is Important for the Coordinated Processive Movement of Kinesin-1. *Biophysical Journal*. 98:369a-369a.

Jumper, J., R. Evans, A. Pritzel, T. Green, M. Figurnov, O. Ronneberger, K. Tunyasuvunakool, R. Bates, A. Zidek, A. Potapenko, A. Bridgland, C. Meyer, S.A.A. Kohl, A.J. Ballard, A. Cowie, B. Romera-Paredes, S. Nikolov, R. Jain, J. Adler, T. Back, S. Petersen, D. Reiman, E. Clancy, M. Zielinski, M. Steinegger, M. Pacholska, T. Berghammer, S. Bodenstein, D. Silver, O. Vinyals, A.W. Senior, K. Kavukcuoglu, P. Kohli, and D. Hassabis. 2021. Highly accurate protein structure prediction with AlphaFold. *Nature*. 596:583-589.

Kita, T., K. Chiba, J. Wang, A. Nakagawa, and S. Niwa. 2024. Comparative analysis of two Caenorhabditis elegans kinesins KLP-6 and UNC-104 reveals a common and distinct activation mechanism in kinesin-3. *Elife*. 12.

Levesque, A.A., and D.A. Compton. 2001. The chromokinesin Kid is necessary for chromosome arm orientation and oscillation, but not congression, on mitotic spindles. *J Cell Biol*. 154:1135-1146.

Li, C., C. Xue, Q. Yang, B.C. Low, and Y.C. Liou. 2016. NuSAP governs chromosome oscillation by facilitating the Kid-generated polar ejection force. *Nat Commun*. 7:10597.

Matthies, H.J., R.J. Baskin, and R.S. Hawley. 2001. Orphan kinesin NOD lacks motile properties but does possess a microtubule-stimulated ATPase activity. *Mol Biol Cell*. 12:4000-4012.

Mirdita, M., K. Schutze, Y. Moriwaki, L. Heo, S. Ovchinnikov, and M. Steinegger. 2022. ColabFold: making protein folding accessible to all. *Nat Methods*. 19:679-682.

Ohsugi, M., N. Tokai-Nishizumi, K. Shiroguchi, Y.Y. Toyoshima, J. Inoue, and T. Yamamoto. 2003. Cdc2-mediated phosphorylation of Kid controls its distribution to spindle and chromosomes.

EMBO J. 22:2091-2103.

Okada, Y., H. Higuchi, and N. Hirokawa. 2003. Processivity of the single-headed kinesin KIF1A through biased binding to tubulin. *Nature*. 424:574-577.

Rieder, C.L., E.A. Davison, L.C. Jensen, L. Cassimeris, and E.D. Salmon. 1986. Oscillatory movements of monooriented chromosomes and their position relative to the spindle pole result from the ejection properties of the aster and half-spindle. *J Cell Biol*. 103:581-591.

Shastry, S., and W.O. Hancock. 2010. Neck linker length determines the degree of processivity in kinesin-1 and kinesin-2 motors. *Curr Biol*. 20:939-943.

Shiroguchi, K., M. Ohsugi, M. Edamatsu, T. Yamamoto, and Y.Y. Toyoshima. 2003. The second microtubule-binding site of monomeric kid enhances the microtubule affinity. *J Biol Chem*. 278:22460-22465.

Soeda, S., K. Yamada-Nomoto, and M. Ohsugi. 2016. The microtubule-binding and coiled-coil domains of Kid are required to turn off the polar ejection force at anaphase. *J Cell Sci*. 129:3609-3619.

Sonn-Segev, A., K. Belacic, T. Bodrug, G. Young, R.T. VanderLinden, B.A. Schulman, J. Schimpf, T. Friedrich, P.V. Dip, T.U. Schwartz, B. Bauer, J.M. Peters, W.B. Struwe, J.L.P. Benesch, N.G. Brown, D. Haselbach, and P. Kukura. 2020. Quantifying the heterogeneity of macromolecular machines by mass photometry. *Nat Commun*. 11:1772.

Soppina, V., S.R. Norris, A.S. Dizaji, M. Kortus, S. Veatch, M. Peckham, and K.J. Verhey. 2014. Dimerization of mammalian kinesin-3 motors results in superprocessive motion. *Proc Natl Acad Sci U S A*. 111:5562-5567.

Stumpff, J., M. Wagenbach, A. Franck, C.L. Asbury, and L. Wordeman. 2012. Kif18A and chromokinesins confine centromere movements via microtubule growth suppression and spatial control of kinetochore tension. *Dev Cell*. 22:1017-1029.

Takagi, J., T. Itabashi, K. Suzuki, and S. Ishiwata. 2013. Chromosome position at the spindle equator is regulated by chromokinesin and a bipolar microtubule array. *Sci Rep*. 3:2808.

Tan, Z., Y. Yue, F. da Veiga Leprevost, S.E. Haynes, V. Basrur, A.I. Nesvizhskii, K.J. Verhey, and M.A. Cianfrocco. 2023. Autoinhibited kinesin-1 adopts a hierarchical folding pattern. *elife*. 12:RP86776.

Thompson, A.F., P.R. Blackburn, N.S. Arons, S.N. Stevens, D. Babovic-Vuksanovic, J.B. Lian, E.W. Klee, and J. Stumpff. 2022. Pathogenic mutations in the chromokinesin KIF22 disrupt anaphase chromosome segregation. *Elife*. 11.

Tokai, N., A. Fujimoto-Nishiyama, Y. Toyoshima, S. Yonemura, S. Tsukita, J. Inoue, and T. Yamamota. 1996. Kid, a novel kinesin-like DNA binding protein, is localized to chromosomes and the mitotic spindle. *EMBO J*. 15:457-467.

Tomishige, M., D.R. Klopfenstein, and R.D. Vale. 2002. Conversion of Unc104/KIF1A kinesin into a processive motor after dimerization. *Science*. 297:2263-2267.

Wandke, C., M. Barisic, R. Sigl, V. Rauch, F. Wolf, A.C. Amaro, C.H. Tan, A.J. Pereira, U. Kutay, H. Maiato, P. Meraldi, and S. Geley. 2012. Human chromokinesins promote chromosome congression and spindle microtubule dynamics during mitosis. *J Cell Biol*. 198:847-863.

Wang, W., J. Ren, W. Song, Y. Zhang, and W. Feng. 2022. The architecture of kinesin-3 KLP-6 reveals a multilevel-lockdown mechanism for autoinhibition. *Nat Commun*. 13:4281.

Weijman, J.F., S.K.N. Yadav, K.J. Surridge, J.A. Cross, U. Borucu, J. Mantell, D.N. Woolfson, C. Schaffitzel, and M.P. Dodding. 2022. Molecular architecture of the autoinhibited kinesin-1 lambda particle. *Sci Adv*. 8:eabp9660.

Wordeman, L. 2010. How kinesin motor proteins drive mitotic spindle function: Lessons from molecular assays. *Semin Cell Dev Biol*. 21:260-268.

Yajima, J., M. Edamatsu, J. Watai-Nishii, N. Tokai-Nishizumi, T. Yamamoto, and Y.Y. Toyoshima. 2003. The human chromokinesin Kid is a plus end-directed microtubule-based motor. *EMBO J*. 22:1067-1074.

Ye, A.A., V. Verma, and T.J. Maresca. 2018. NOD is a plus end-directed motor that binds EB1 via a new microtubule tip localization sequence. *J Cell Biol*. 217:3007-3017.

Yildiz, A., M. Tomishige, A. Gennerich, and R.D. Vale. 2008. Intramolecular strain coordinates kinesin stepping behavior along microtubules. *Cell*. 134:1030-1041.

Figure legends

Figure 1 Kid is a processive motor

(A) Schematic illustration of the domain organization in Xenopus Kid tagged with a fluorescent protein mScarlet (XKidFL) and human Kid tagged with mNeonGreen (hKidFL). The calculated molecular weights of the fusion proteins are indicated on the right.

(B) Representative SDS-PAGE analysis of purified XKidFL and hKidFL fusion proteins. The proteins are visualized using a Stain-Free gel. The molecular weight standards are indicated on the left side of the SDS-PAGE images.

(C and D) Representative kymographs showing the motility of XKidFL at 20 pM (C) and hKidFL at 20 pM (D) both in the presence of 2 mM ATP. Scale bars: horizontal, 10 µm; vertical, 60 seconds.

(E) Dot plots showing the velocity of XKidFL and hKidFL. Each dot shows a single datum point. Green bars represent mean ± S.D.. n = 71, respectively.

(F) Dot plots showing the run length of XKidFL and hKidFL. Each dot shows a single datum point. Green bars represent mean ± S.D.. n = 70, respectively.

Figure 2 Kid forms a weak dimer

(A) Size exclusion chromatography profiles of hKidFL (black) and UNC-104(1-653)-sfGFP (cyan). Below the chromatography, an SDS-PAGE image show the elution fractions. Asterisks indicate

fractions used for mass photometry and single molecule assays. The molecular weight standards are indicated on the left side of the SDS-PAGE images.

(B) Size exclusion chromatography of XKidFL (black) and UNC-104(1-653) (cyan). The SDS-PAGE of the elution fractions are shown beneath the profiles. Asterisks indicate fractions used for mass photometry and single molecule assays. The number shown at the left side indicates molecular weight standard.

(C) Mass photometry of human Kid. Histograms show the number of counts at 5 nM. Lines show Gaussian fits (mean ± S.D.: 110 ± 21 kDa and 211 ± 21 kDa, respectively).

(D) Mass photometry of Xenopus Kid. Histograms show the number of counts at 5 nM. Lines show Gaussian fits (mean ± S.D.: 117 ± 33 kDa and 208 ± 49 kDa, respectively).

Note that majority of hKid and XKid are dimers in the size exclusion chromatography but they are mostly dissociated to monomers in mass photometry.

Figure 3 Conserved coiled-coil domain is required for the processive motion

(A) Schematic representation illustrating the domain organization of XKid(1-495) and XKid(1-437).

(B) Representative SDS-PAGE analysis of purified XKid(1-495) and XKid(1-437) proteins. The proteins are visualized using a Stain-Free gel. The molecular weight standards are indicated on the right side of the SDS-PAGE images.

(C and D) Representative kymographs showing the motility of 20 pM XKid(1-495) (C) and XKid(1-437) (D) in the presence of 2 mM ATP. Note that no directional movement was detected in XKid(1-437). Scale bars: horizontal 5 µm; vertical 60 seconds.

(E) Dot plots showing the velocity of XKid(1-495) and XKid(1-437). Each dot represents an individual measurement of velocity. Green bars represent mean ± S.D.. n= 57 particles for XKid(1-495). nd, not detected.

(F) Dot plots showing the run length of XKid(1-495) and XKid(1-437). Each dot shows a single datum point. Green bars represent mean ± S.D.. n = 57 particles for XKid(1-495). nd, not detected.

(G and H) Schematic drawing of XKidCC-mScarlet (G) and a representative result of size exclusion chromatography (H). XKidCC-mScarlet (magenta) and mScarlet (cyan) are shown.

Figure 4 Untypical neck linker of Kid can support processive movement of KIF1A

(A) Schematic representation illustrating the domain organization of KIF1A(1-393)LZ, XKid(1-495), KIF1A(1-350) and a chimera protein KIF1AMD-XKidSt. Note that KIF1A(1-393)LZ and XKid(1-495) are processive motors and KIF1A(1-350) is a non-processive motor. Cyan, motor domain of KIF1A; Orange, motor domain of Kid; Magenta, neck linker.

(B) Amino acid sequences of the neck linker region. KIF1A, XKid, hKid, KIF5C and KIF1AMD-XKidSt are shown. Cyan, motor domain of KIF1A and KIF5C; Orange, motor domain of

Kid; Magenta, neck linker; Green, neck coiled-coil domain.

(C) Representative SDS-PAGE analysis of purified KIF1AMD-XKidSt fusion protein. The protein is visualized using a Stain-Free gel. The molecular weight standards are indicated on the right side of the SDS-PAGE image.

(D and E) Representative kymographs showing the motility of KIF1AMD-XKidSt and KIF1A(1-393)LZ in the presence of 2 mM ATP. Note that KIF1AMD-XKidSt exhibits diffusion-like fluctuations while they are moving. This phenomena is not observed in KIF1A(1-393)LZ. Scale bars: horizontal 10 µm; vertical 10 seconds.

(F) Dot plots showing the velocity of KIF1AMD-XKidSt and KIF1A(1-393)LZ. Each dot shows a single datum point. Green bars represent mean ± S.D.. ****, $p < 0.0001$, Unpaired t-test. n = 273 and 434 particles for KIF1AMD-XKidSt and KIF1A(1-393)LZ, respectively.

(G) Dot plots showing the run length of KIF1AMD-XKidSt and KIF1A(1-393)LZ. Each dot shows a single datum point. Green bars represent median value and interquartile range. ****, $p < 0.0001$, Mann-Whitney test. n = 273 and 434 particles for KIF1AMD-XKidSt and KIF1A(1-393)LZ, respectively.

Figure 5 DNA movement driven by XKid

1nM of XKid fused with sfGFP and 20 nM of Cy3 labelled double-strand or single-strand DNA were mixed and observed under the TIRF microscopy.

(A-C) Representative kymographs showing the movement of full-length XKid and double-strand DNA (A), full-length XKid and single-strand DNA (B) and XKid(1-495) and double-strand DNA.

Scale bars: horizontal, 10 µm; vertical, 60 seconds.

(D) A dot plot showing the frequency of DNA movement along microtubules, normalized by microtubule length (1 µm) and observation time window (1 minute). Each dot represents an individual measurement obtained from observations of different microtubules. N = 22, 10 and 35 microtubules, respectively.

Figure 6 Model

Kid forms dimers and transports chromosomes along prometaphase spindle microtubules by directly binding with genomic DNA.

Supplemental Movie legends

Movie S1

The motility of XKid was analyzed through time-lapse imaging recorded at 0.5 frames per second (fps) and played back at 25 fps. The dimensions of the displayed frame are 30 µm by 7 µm.

Movie S2

The motility of hKid was analyzed through time-lapse imaging recorded at 0.5 fps and played back at 25 fps. The dimensions of the displayed frame are 30 µm by 7 µm.

Movie S3

The motility of KIF1AMD-XKidSt was analyzed through time-lapse imaging recorded at 10 fps and played back at 25 fps. The dimensions of the displayed frame are 30 µm by 7 µm.

Movie S4

The motility of KIF1A(1-393)LZ was analyzed through time-lapse imaging recorded at 10 fps and played back at 25 fps. The dimensions of the displayed frame are 30 µm by 7 µm.

Movie S5

The motility of hKid-mNeonGreen (Green) and Cy3 labelled double-strand DNA (Red) was observed through time-lapse imaging recorded at 0.5 fps and played back at 10 fps. The dimensions of the displayed frame are 25 µm by 8 µm.

	Processive	Oligomeric state in SEC	Velocity (µm/sec)	Run length (µm)
Full length hKid	Yes	Dimer	0.0671 ± 0.0319	4.11 ± 2.27
Full length XKid	Yes	Dimer	0.0646 ± 0.0247	3.67 ± 2.16
XKid(1-495)	Yes	Dimer	0.0646 ± 0.0266	4.18 ± 1.56
XKid(1-437)	No	Monomer	nd	nd
KIF1A(1-393)LZ	Yes	Dimer	1.37 ± 0.44	11.1 ± 10.9
KIF1AMD-XKidSt	Yes	Dimer	0.67 ± 0.18	6.67 ± 6.02

Table 1 Motile properties of constructs used in this study

Motor protein constructs underwent purification through affinity chromatography followed by size exclusion chromatography, as detailed in the Materials and Methods section. The reported velocities and run lengths represent mean values ± standard deviation (SD). Notably, XKid(1-437) failed to demonstrate consistent processive motion across three separate protein preparations, indicating a lack of detectable activity (ND: not detected).

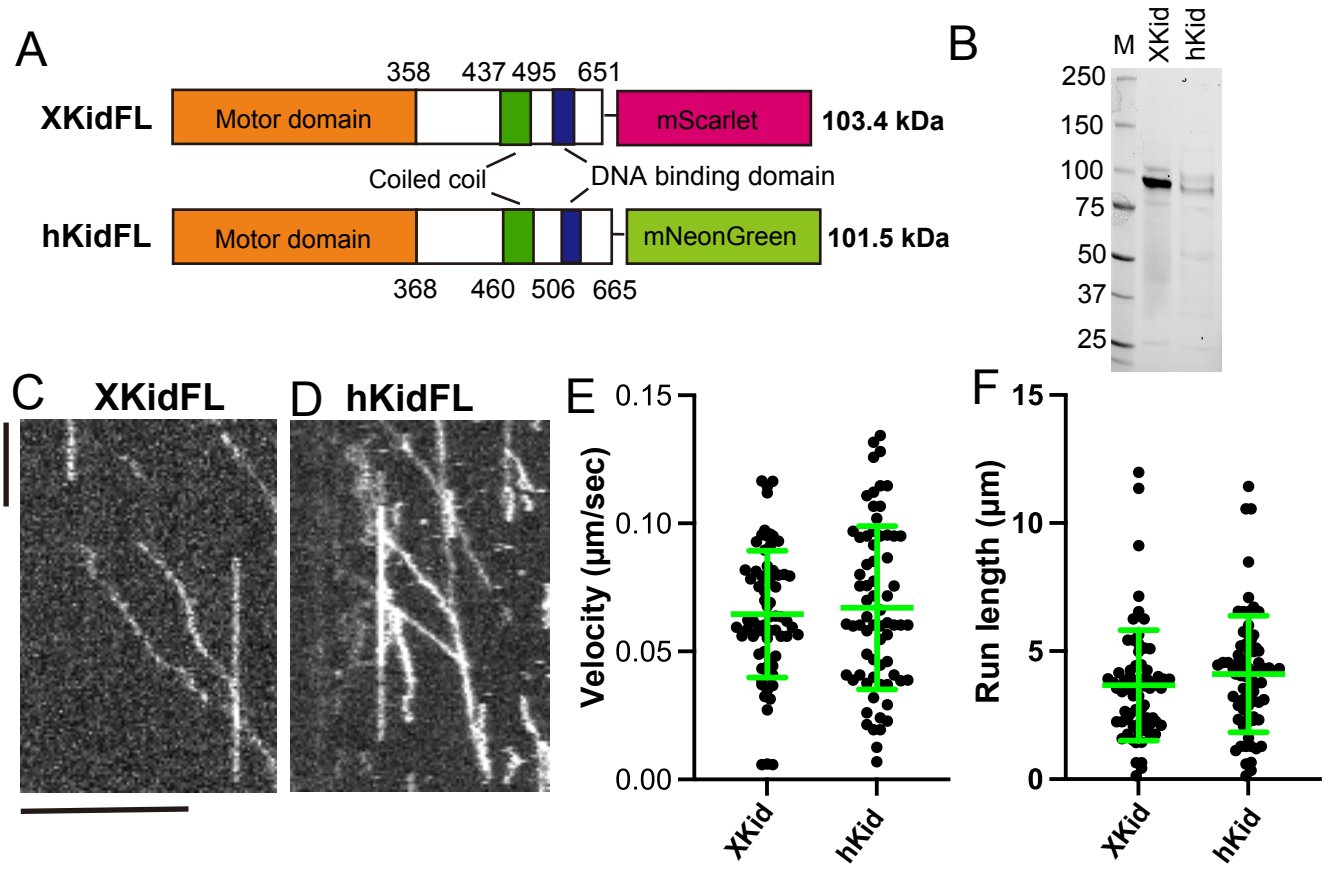

Niwa and Furusaki et al. Figure 1

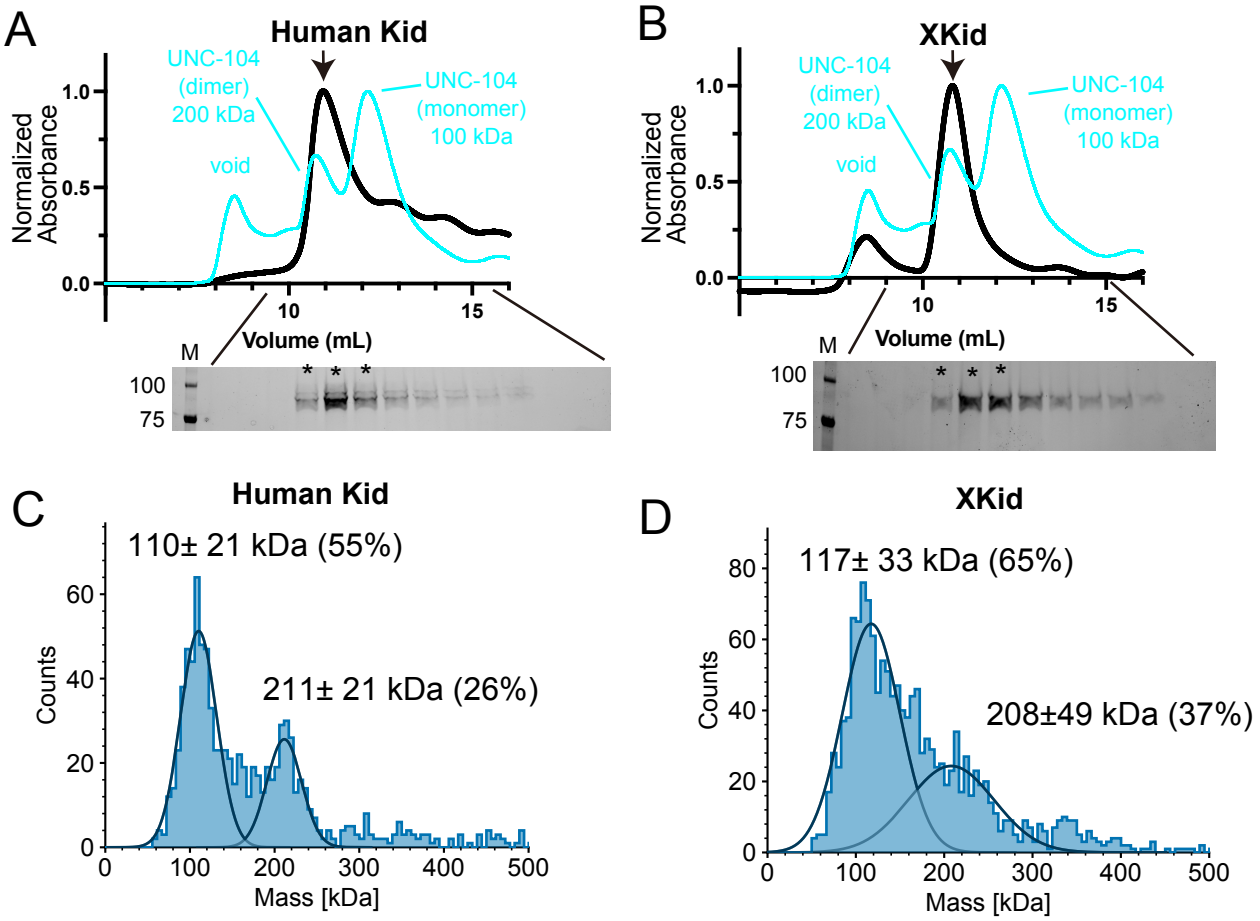

Niwa and Furusaki et al. Figure 2

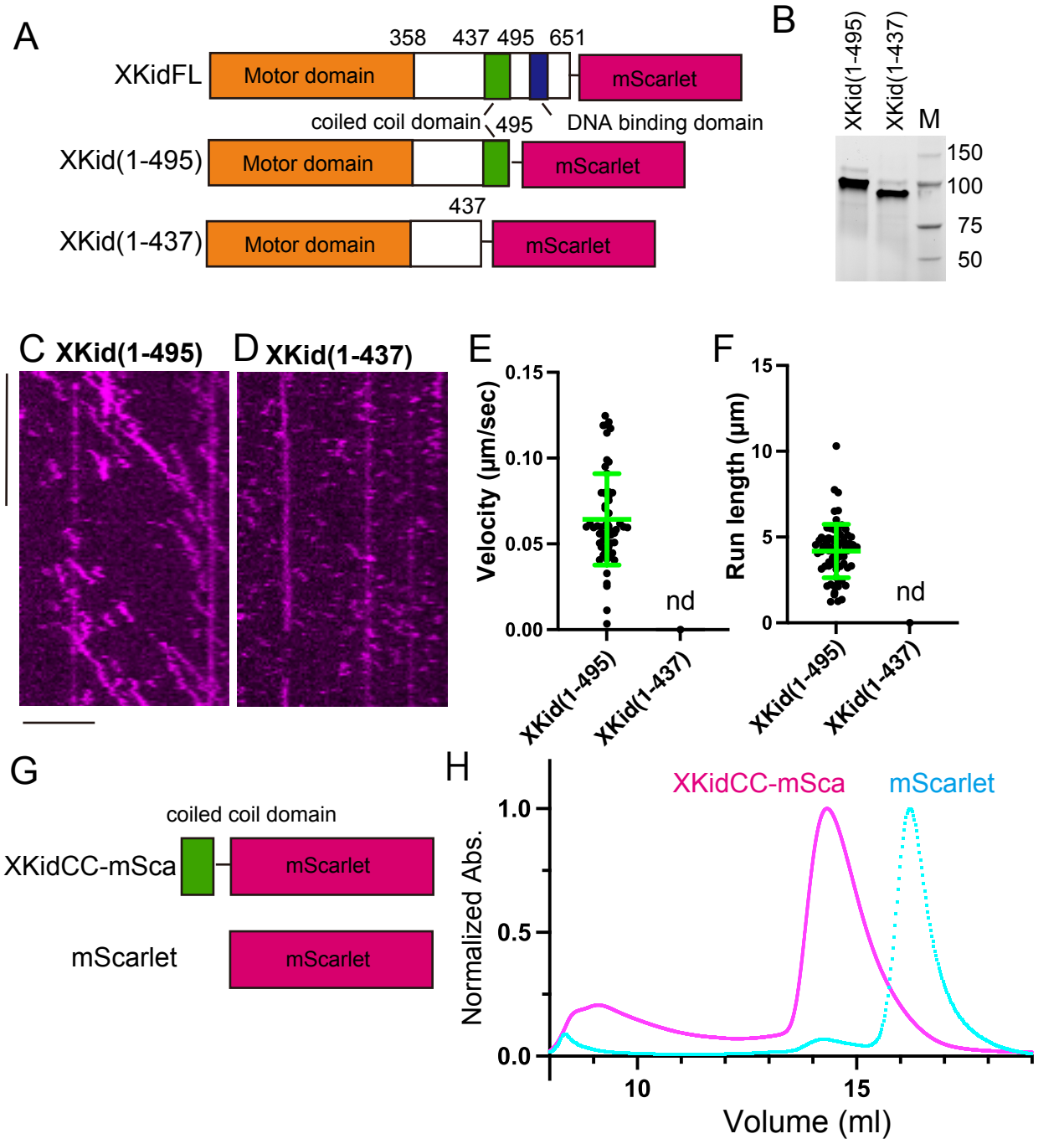

Niwa and Furusaki et al. Figure 3

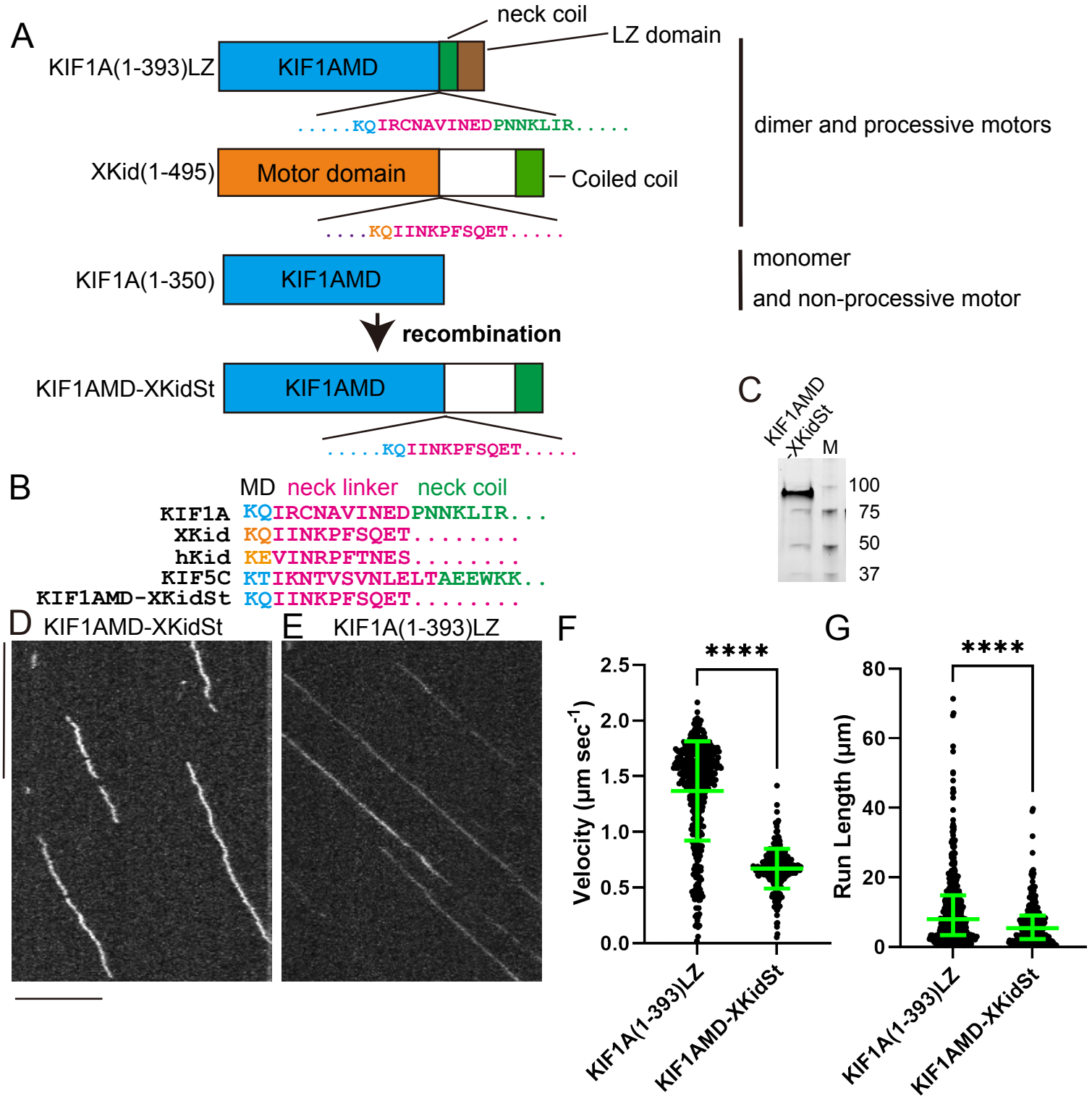

Niwa and Furusaki et al. Figure 4

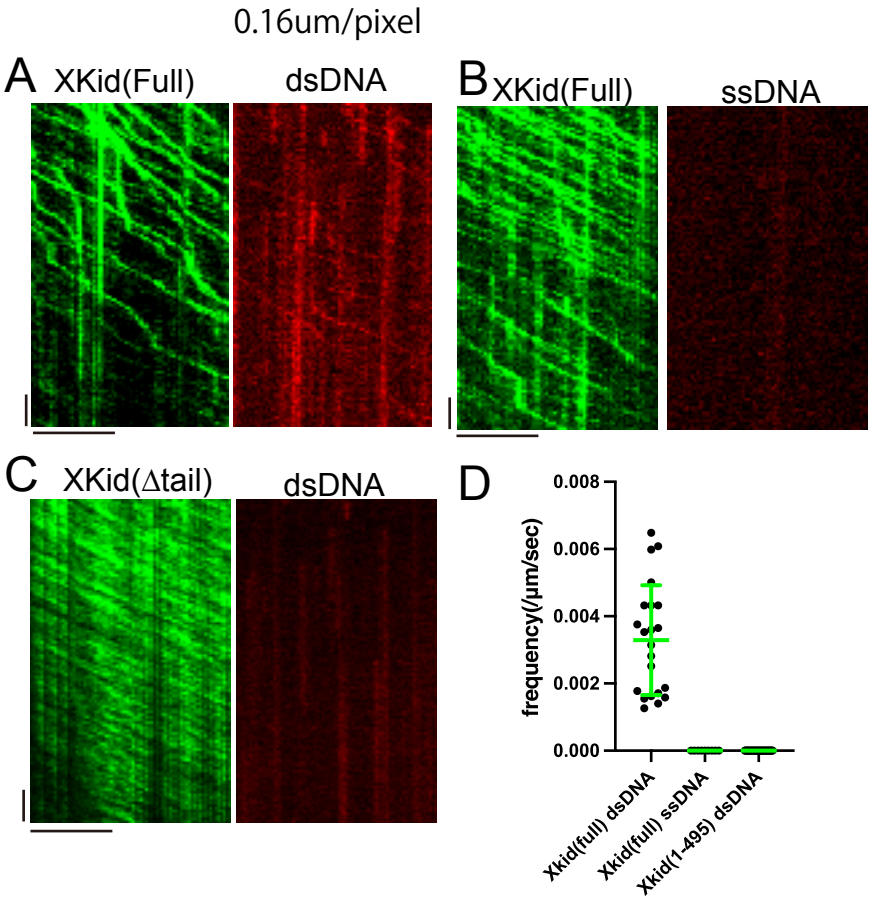
0.16um/pixel
A
XKid(Full)
dsDNA
B
XKid(Full)
ssDNA
C
XKid(Δtail)
dsDNA
D
frequency(/μm/sec)
0.008
0.006
0.004
0.002
0.000
Xkid(full) dsDNA
Xkid(full) ssDNA
Xkid(1-495) dsDNA

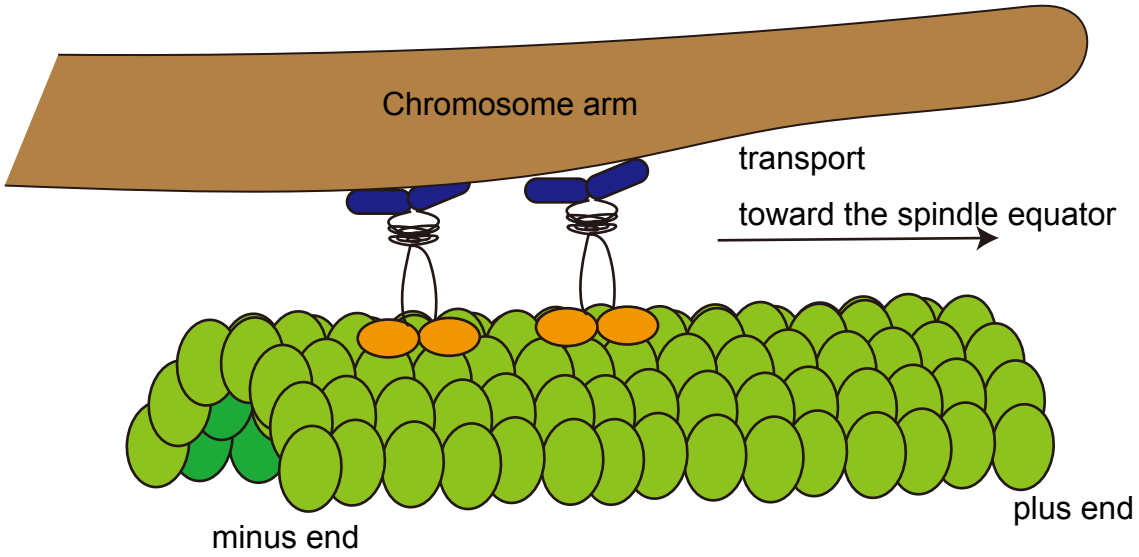

Niwa and Furusaki et al. Figure 6